

Original Investigation

Simulated Effects of Perianeurysmal Bone on a Cerebral Aneurysm: A Case Study

Fuyu WANG*, Zhe XUE*, Zhenghui SUN, Jinli JIANG, Chen WU, Bainan XU

Chinese PLA General Hospital, Department of Neurosurgery, Beijing, China

*Fuyu WANG and Zhe XUE contributed equally to the work.

ABSTRACT**AIM:** To use computational models to explore the influence of contact with perianeurysmal bone on an intracranial aneurysm.**MATERIAL and METHODS:** A middle cerebral artery aneurysm in contact with an anterior clinoid process was selected. Two anatomic models were constructed from computed tomography angiography images: A non-contact model with elasticity of the entire aneurysm wall and a contact model with rigidity of the part of the aneurysm wall contacting bone. The blood flow pattern, and wall stress and displacement were compared between the two models.**RESULTS:** The contact and non-contact models exhibited similar wall shear stress and pressure, but different degrees of von Mises stress and wall displacement. Displacement close to the bone contact part of the aneurysm wall was less in the contact model than in the non-contact model, whereas displacement of the part opposite to the contact part was larger in the contact model than in the non-contact model. Also, von Mises stress close to the contact part was larger in the contact model than in the non-contact model.**CONCLUSION:** Contacting perianeurysmal bone affects the deformation and degree of von Mises stress but not the hemodynamics of intracranial aneurysms.**KEYWORDS:** Aneurysm, Deformation, Hemodynamic, Perianeurysmal bone, Stress**INTRODUCTION**

Intracranial aneurysm rupture is a cause of subarachnoid hemorrhage that results in substantial rates of morbidity and mortality. To treat intracranial aneurysms more effectively, it is important to have a better understanding of their natural history. The flow dynamics is important in the origination and development of cerebral aneurysms. Computational models can be used to study intra-aneurysmal hemodynamics resulting from any possible geometry (7,8), allowing prediction of possible aneurysm growth and rupture (2).

As the walls of blood vessels and aneurysms are elastic, both their pulsatile motion and mechanical properties influence aneurysm rupture, indicating that fluid-solid interaction (FSI) should be an important consideration (3). However, the aneurysm wall is living, continuously re-modeled tissue that

often exhibits varied thickness that is difficult to accurately measure. The walls of growing aneurysms can also develop atherosclerosis, making it difficult to assess their mechanical properties. As non-invasive computed tomography angiography (CTA) has recently been used as an alternative to 3D digital subtraction angiography to detect cerebral aneurysms (1), CTA images could be used to construct computational anatomical models for investigating aneurysmal hemodynamics and wall properties.

Most aneurysms are located in the subarachnoid space, meaning that perianeurysmal structures such as bone, brain parenchyma, cerebrospinal fluid, and arachnoid chordae and membranes can affect aneurysm evolution. Due to differences in the material properties of various perianeurysmal structures, it is difficult to simulate multifactorial interactions in a simplified computational model. However, as bone may exert an undue



Corresponding author: Zhenghui SUN

E-mail: wangfytxdy@126.com

influence on aneurysm deformation and growth, the wall of aneurysms could be considered to consist of two parts: a rigid part that makes contact with bone and an elastic part that does not make contact with bone. Therefore, in the present study, we constructed and compared two models—a contact model and a non-contact model—to examine the effects of perianeurysmal structures on aneurysm hemodynamics and wall properties.

■ MATERIAL and METHODS

CTA

CTA (Figure 1A) was performed using a helical computed tomography (CT) scanner (LightSpeed 16; GE Medical Systems) with multidetector-row capability. Data were obtained using a section thickness of 0.625 mm and a table speed of 9 mm/s (120 kV, 315 mAs). Zero-degree table and gantry tilt were used. Sections in DICOM format were acquired with a 512×512 matrix. Scanning started at the C1 level and continued cranially parallel to the orbitomeatal line ending at the skull vertex during the intravenous injection of contrast material at a rate of 3.5 mL/s.

Digital images and accompanying files were directly imported into MIMICS software to construct 3D models. The luminal surface of blood vessels was extracted in a format suitable for import by grid generators.

MIMICS Software

MIMICS 10.0 software (Materialise, Leuven, Belgium) was used to define the region of interest (ROI) (Figure 1B) and to extract the luminal vascular surface from the previously obtained 3D raster gray-scale image. To visualize the contact area between the aneurysm and bone, the interface between the wall and bone was marked in green on the axial image. Using the MIMICS Remesh command, we performed automated mesh optimization for computational fluid dynamics (CFD) analysis and exported the file in .lis format. In this manner, we generated both a fluid model (blood flow) and a solid model (wall). The .lis file was converted to an IGES file by ANSYS software as a geometry input format used by most modern commercial grid generators.

Construction of Contact and Non-contact Models

The contact and non-contact models had the same fluid model and different types of solid models. In the contact model, the solid model was separated into two parts in the DesignModeler module of Workbench, with the part of the wall contacting bone assigned a steel property with a Young modulus of 2×10^5 Mpa and a Poisson's ratio of 0.3 and the part of the wall not contacting bone assigned an artery property with a Young modulus of 2.7 Mpa and a Poisson's ratio of 0.45 in the Simulation module of Workbench. In the non-contact model, the entire wall was assigned an artery property with similar constants as those in the contact model.

Workbench 11.0 software was used to generate the grid. The number of grid nodes was chosen as a reasonable compromise between accuracy and computational time of

subsequent simulations. Mesh independence was performed to determine the optimal number of elements.

Numerical Modeling

For hemodynamic analysis, blood flow was assumed to be laminar and Newtonian. Incompressible Navier-Stokes equations were used as the governing equations, which are suitable for problems with FSI. Numerical modeling was performed using commercially available ANSYS-CFX11 software. The inlet boundary condition was set by specifying velocity at the inlet. Blood density was set at 1050 kg/m^3 .

For structural analysis, numerical modeling was performed using commercially available ANSYS-Mechanical software. The momentum conservation equation was used as the governing equation.

■ RESULTS

The anatomic models (Figure 1C) showed the point of contact between the aneurysm wall and bone in green (Figure 1D). The part of the aneurysm wall contacting bone showed almost no deformation in the contact model (darker blue; Figure 2A), and the neighboring wall showed less deformation in the contact model (darker blue) than in the non-contact model (lighter blue; Figure 2C). The aneurysm wall opposite from the contact part showed more deformation in the contact model (darker red; Figure 2B) than in the non-contact model (lighter red; Figure 2D). Across the 15 points marked along the aneurysm wall (Figures 2A-D), points 5 and 6 were located on the contact part, points 1 to 4 were located to the left of

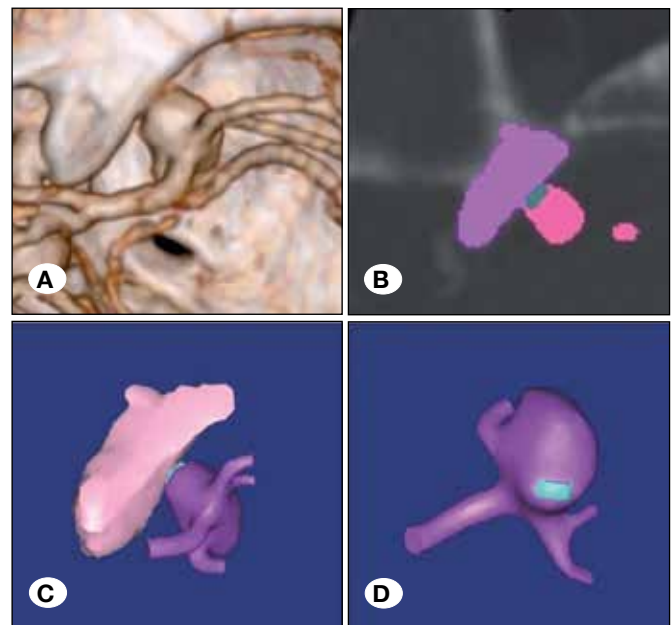


Figure 1: CTA image of a right middle cerebral aneurysm contacting an anterior clinoid process (A). The point of contact between the aneurysm and bone was marked in green (B). 3D construction of the aneurysm and anterior clinoid process (C), with green marking the bone contact part of the aneurysm wall (D).

the contact part, points 7 to 9 were located to the right of the contact part, and points 10 to 15 were located opposite to the contact part. The displacement of points 5 and 6 was lower in the contact model than in the non-contact model (Figure 6A), indicating that bone contact constrained wall movement. By contrast, the displacement of points 14 and 15 was higher in the contact model than in the non-contact model, indicating that bone contact led to greater deformation of the opposite wall.

The contact part and neighboring wall showed higher von Mises stress in the contact model (lighter blue; Figure 3A) than in the non-contact model (darker blue; Figure 3C), whereas the opposite wall showed similar degrees of stress between the two models (Figures 3B, D). The von Mises stress of points 5 to 7 was higher in the contact model than in the non-contact model (Figure 6B), indicating that bone contact increased stress on the aneurysm wall. Furthermore, the presence of differences in von Mises stress at other points between the two models suggest the complicated nature of changes in aneurysm wall stress resulting from bone contact.

No differences in wall total pressure (Figures 4A-D, 6C) or wall shear stress (Figures 5A-D, 6D) were found between the contact and non-contact models.

DISCUSSION

As an aneurysm becomes larger, it can displace soft tissues

such as nerves, arteries, and brain tissues and can even erode bone. On the other hand, perianeurysmal structures can constrain aneurysm growth. Whereas the effects of soft tissue on aneurysms can be difficult to simulate with the CFD technique, the effects of rigid bone on aneurysms can be more easily simulated. However, due to the complexity of combining both rigid and FSI models in a single computational model, we employed an FSI model in which different parts of the aneurysm wall had different material properties (i.e., a steel property was assigned to the part of the wall contacting bone). We observed that deformation of the aneurysm wall was lower at the contact part and neighboring areas in the contact model than in the non-contact model, indicating that the contact model reasonably simulated the effect of bone on the aneurysm. Furthermore, deformation of the wall opposite from the contact part was larger in the contact model than in the non-contact model, suggesting displacement of the aneurysm wall in response to bone contact. Therefore, when aneurysms grow and contact bone, enlargement of the wall is constrained at and around the point of contact but may become more pronounced opposite to the side of contact. In our case, however, no further follow-up was performed to examine changes in aneurysm shape because the aneurysm was clipped. Other study has reported similar observations of the effect of perianeurysmal bone on the growth of cerebral aneurysms (9). After 4 years of follow-up of a large aneurysm of the basilar artery that made contact with bone,

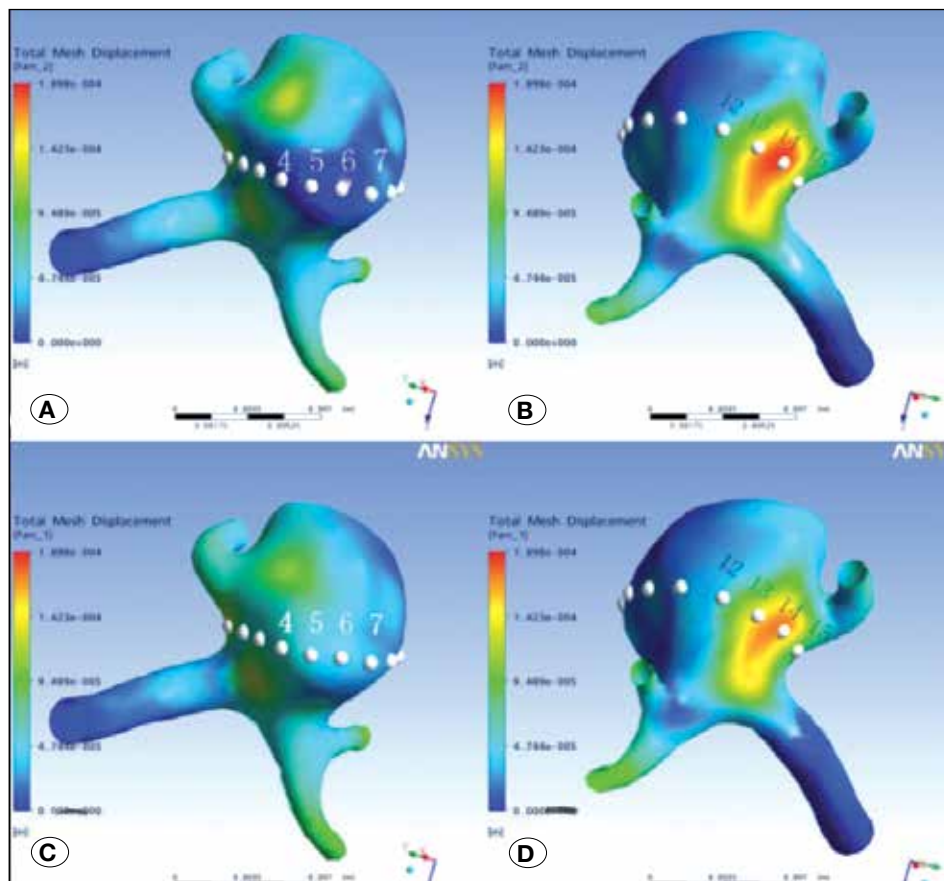


Figure 2: Images of aneurysm wall total mesh displacement for the contact model (A, B), and non-contact model (C, D). Red indicates high mesh displacement, and blue indicates low mesh displacement.

Sforza et al. showed that the aneurysm pushed against the bone and deformed in the opposite (i.e., right/posterior) direction, causing displacement of the parent artery in the right/posterior direction and altering its curvature immediately proximal to the vertebral artery junction and the aneurysm (9). Thus, contacting bone can change the direction of growth of aneurysms.

The von Mises criterion suggests that the yielding of materials begins when the stress reaches a critical value known as yield strength. Thus, von Mises stress can be used to predict the rupture of aneurysms. A previous study shows that the von Mises stress of an abdominal aortic aneurysm wall is closely related to its specific geometry and that abdominal aortic aneurysms can have different stress distributions with

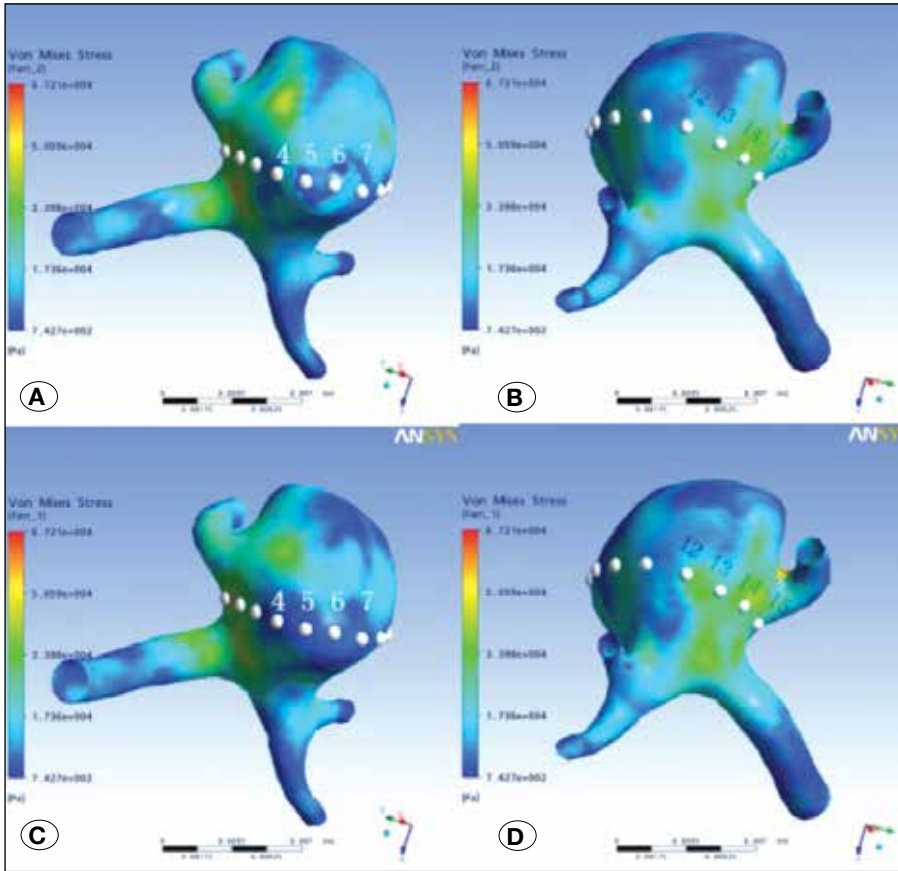


Figure 3: Images of aneurysm wall von Mises stress for the contact model (A, B), and non-contact model (C, D). Red indicates high von Mises stress, and blue indicates low von Mises stress.

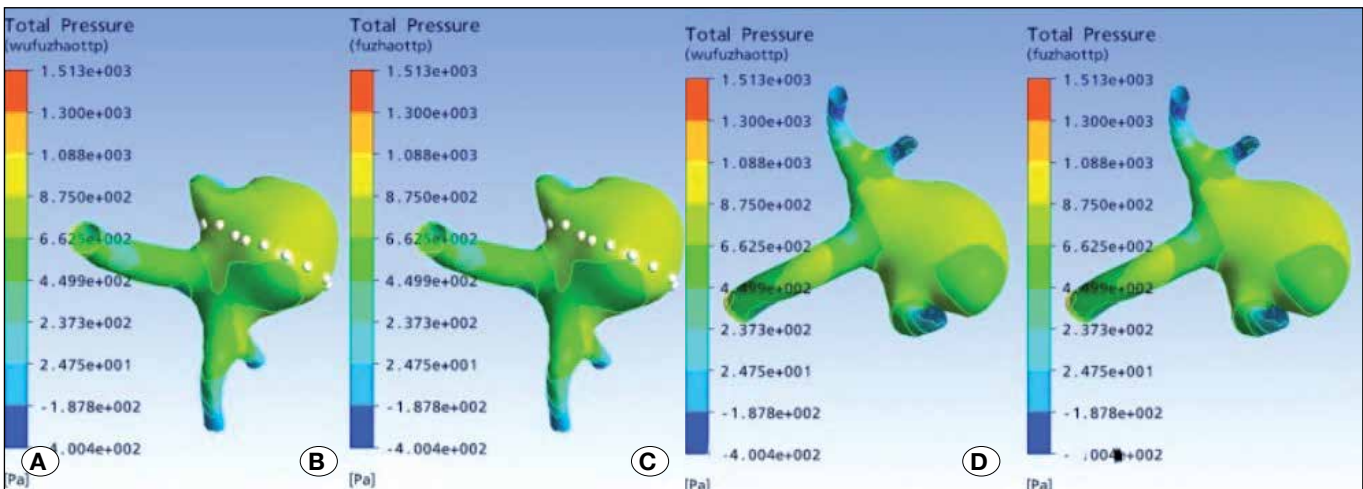


Figure 4: Images of aneurysm wall total pressure for the contact model (B, D), and non-contact model (A, C). Red indicates high wall total pressure, and blue indicates low wall total pressure.

equivalent diameters and pressures (11). The present study shows that von Mises stress on the bone contact part of the aneurysm wall was higher in the contact model than in the non-contact model. For the non-contacting part of the aneurysm wall, however, there were different and irregular patterns of spread of von Mises stress between the two

models, suggesting that bone contact with an aneurysm can result in complex changes in von Mises stress.

Wall shear stress is a flow-induced stress resulting from the frictional force of viscous blood. There is increasing evidence that wall shear stress plays a role in the evolution of aneurysmal

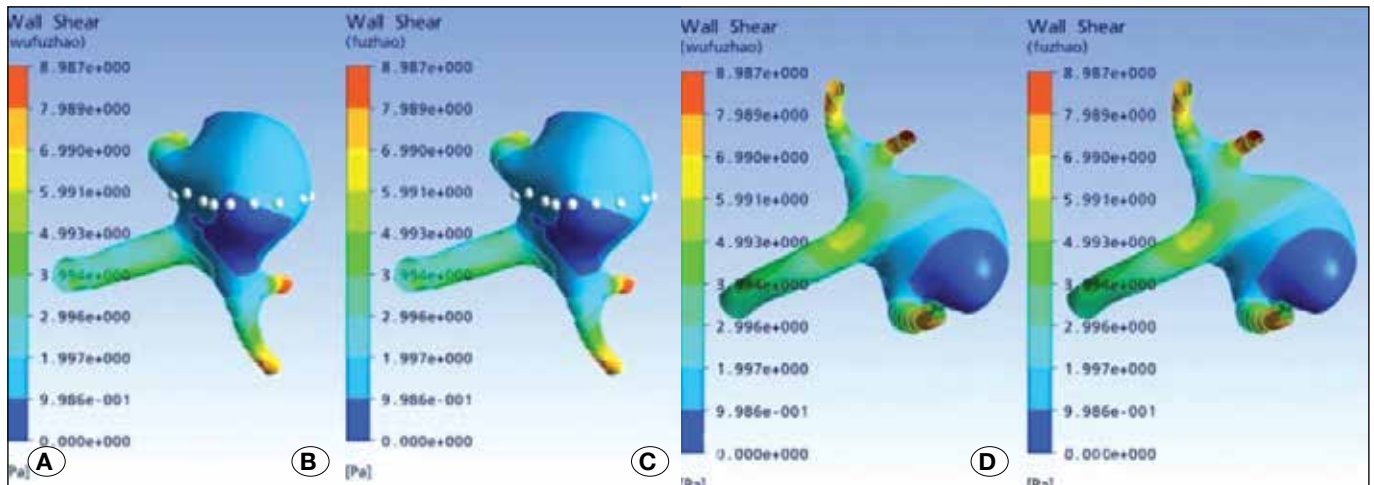


Figure 5: Images of aneurysm wall shear stress for the contact model (B, D), and non-contact model (A, C). Red indicates high wall shear stress, and blue indicates low wall shear stress.

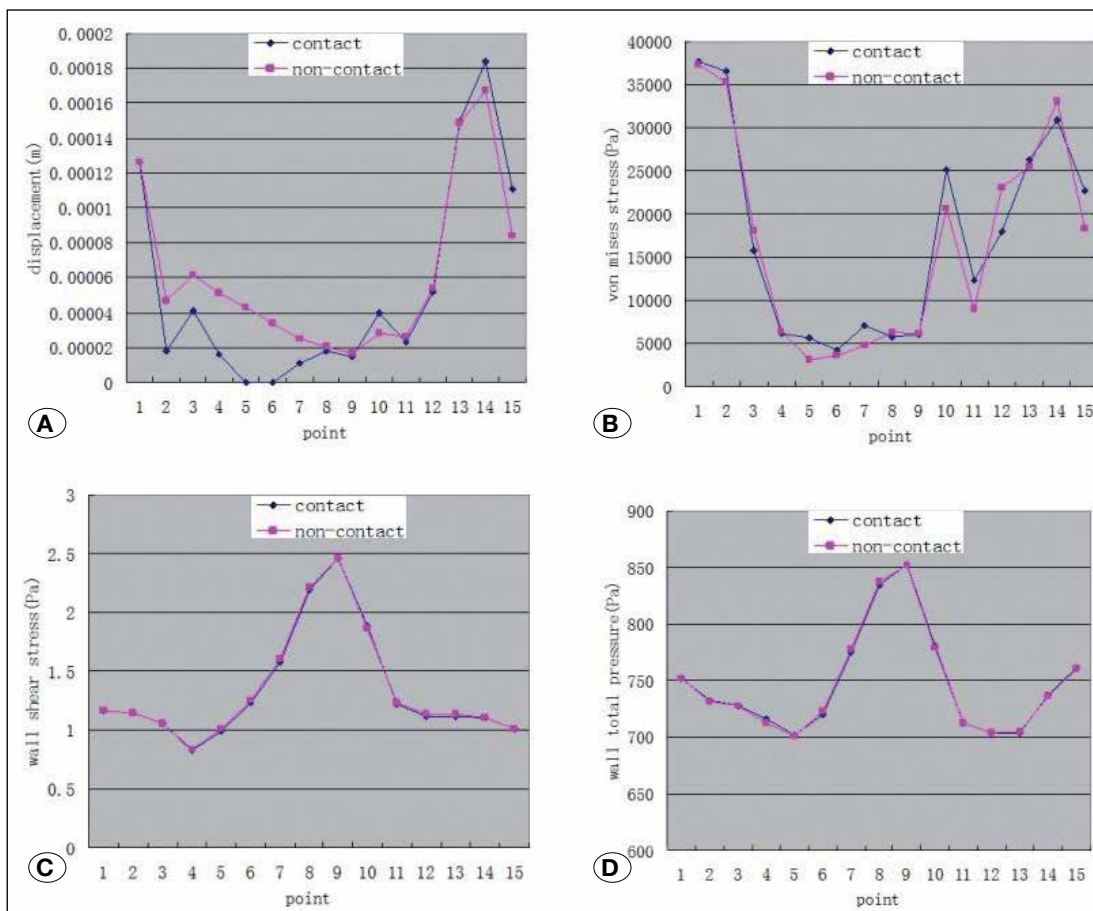


Figure 6: Displacement values (A), von Mises stress (B), wall shear stress (C), and wall total pressure (D) across the 15 points for the contact and non-contact models.

disease, probably through affecting endothelial cell function and gene expression as well as cell shape and structure. Not only can the size and tapering of the internal carotid artery influence wall shear stress, resulting in higher wall shear for small arteries and lower wall shear for large arteries, the size of an aneurysm also influences its wall shear stress. In a previous report, Jou et al. described high wall shear stress at the region where blood entered the aneurysm and lower wall shear stress in the other regions of the aneurysm (6). Tatushima et al. reported that wall shear stress decreased in the deeper part of the bleb in a pre-growth model and decreased even further after aneurysm growth (10). Wang et al. showed that that low wall shear stress may be associated with the initiation and growth of aneurysms and that aneurysm formation and growth may influence hemodynamic parameters in nearby arteries (12). Cebal et al. reported that aneurysm rupture may be caused by localized degradation and weakening of the wall in response to abnormal hemodynamics (4). Also, Ivanov et al. demonstrated that the size and shape of an aneurysm significantly impacts blood flow through the affected vessel and the effective stress distribution across the aneurysm dome (5). In the present study, we found no difference in wall shear stress between contact and non-contact models, suggesting that although bone contact displaced part of the aneurysm wall, this change in geometry was not sufficient to alter wall shear stress.

Blood vessels are also exposed to other forces induced by pulsatile blood flow, such as hydrostatic pressure and dynamic pressure. Hydrostatic pressure is nearly equivalent to blood pressure, whereas dynamic pressure is the force produced when the circulating blood flow impinges on the arterial wall and is superimposed on the hydrostatic pressure. However, as dynamic pressure is very small compared with normal blood pressure, wall pressure may not critically influence aneurysm growth. In the present study, we found no change in pressure between the contact and non-contact models.

To our knowledge, this study is the first to examine the effect of perianeurysmal bone on a cerebral aneurysm using the CFD technique. We found that wall displacement and von Mises stress differed between the contact and non-contact models, but there was no difference in wall shear stress or wall total pressure between models. These findings add to our understanding of the relationship between aneurysms and their environment and how this relationship influences the growth of a cerebral aneurysm. Recently, more centers have been using CTA imaging instead of catheter angiography for preoperative planning. Here, we show that this technique can be used to obtain perianeurysmal bony structure data for simulation studies, as the presence of perianeurysmal structures may more accurately predict the development of aneurysms than angiographic shape.

The results of our study may be limited by several considerations, such as our simplified assumption that blood is a Newtonian fluid and our neglect of the effects of gravity and position. The validity of these assumptions seems to be of secondary importance compared with the influence of aneurysmal geometry. The bone contact part of the aneurysm

wall was assigned a steel property to simulate an undeformed wall, thereby making the model simple to construct with reasonable results. If we could have followed up this case, we could have compared the shape of the aneurysm at different stages of its evolution and verified these changes against our simulation results; however, this will require future work.

■ CONCLUSION

Perianeurysmal bone influences the deformation and von Mises stress of an aneurysm, but may not change wall shear stress or wall total pressure.

■ REFERENCES

1. Anderson GB, Steinke DE, Petruk KC, Ashforth R, Findlay JM: Computed tomographic angiography versus digital subtraction angiography for the diagnosis and early treatment of ruptured intracranial aneurysms. *Neurosurgery* 45:1315-1322, 1999
2. Asari S, Ohmoto T: Natural history and risk factors of unruptured cerebral aneurysms. *Clin Neurol Neurosurg* 95:205-214, 1993
3. Bai-Nan X, Fu-Yu W, Lei L, Xiao-Jun Z, Hai-Yue J: Hemodynamics model of fluid-solid interaction in internal carotid artery aneurysms. *Neurosurg Rev* 34:39-47, 2011
4. Cebal JR, Vazquez M, Sforza DM, Houzeaux G, Tatushima S, Scrivano E, Bleise C, Lylyk P, Putman CM: Analysis of hemodynamics and wall mechanics at sites of cerebral aneurysm rupture. *J Neurointerv Surg* 7:530-536, 2015
5. Ivanov D, Dol A, Polienko A: Patient-specific hemodynamics and stress-strain state of cerebral aneurysms. *Acta Bioeng Biomech* 18:9-17, 2016
6. Jou LD, Wong G, Dispensa B, Lawton MT, Higashida RT, Young WL, Saloner D: Correlation between luminal geometry changes and hemodynamics in fusiform intracranial aneurysms. *AJNR Am J Neuroradiol.* 26:2357-2363, 2005
7. Sforza DM, Kono K, Tatushima S, Viñuela F, Putman C, Cebal JR: Hemodynamics in growing and stable cerebral aneurysms. *J Neurointerv Surg* 8:407-412, 2016
8. Sforza DM, Putman CM, Cebal JR: Computational fluid dynamics in brain aneurysms. *Int J Numer Method Biomed Eng* 28:801-808, 2012
9. Sforza DM, Putman CM, Tatushima S, Viñuela F, Cebal JR: Effects of perianeurysmal environment during the growth of cerebral aneurysms: A case study. *AJNR Am J Neuroradiol* 33:1115-1120, 2012
10. Tatushima S, Tanishita K, Omura H, Villablanca JP, Vinuela F: Intra-aneurysmal hemodynamics during the growth of an unruptured aneurysm: In vitro study using longitudinal CT angiogram database. *AJNR Am J Neuroradiol* 28: 622-627, 2007
11. Vorp DA, Raghavan ML, Webster MW, Pittsburgh P: Mechanical wall stress in abdominal aortic aneurysm: Influence of diameter and asymmetry. *J Vasc Surg* 27:632-639, 1998
12. Wang F, Xu B, Sun Z, Wu C, Zhang X: Wall shear stress in intracranial aneurysms and adjacent arteries. *Neural Regen Res* 8:1007-1015, 2013